When is cloud condensation nuclei activity sensitive to particle characteristics at emission?

Laura Fierce,[1] Nicole Riemer,[2] and Tami C. Bond[1]

Received 25 July 2013; revised 19 November 2013; accepted 22 November 2013; published 17 December 2013.

[1] The cloud condensation nuclei (CCN) activity of an aerosol population depends on individual particles' size and composition. However, these properties are modified shortly after emission by condensation of semivolatile substances and coagulation with other particles. It is, therefore, unclear to what extent particle characteristics at emission affect CCN activity after aging by condensation and coagulation. We present a process-level analysis of particles emitted from a particular source, diesel engines, in which we isolate the separate effects of condensation and coagulation on the CCN activation of primary aerosol. We simulated aerosol dynamics in a polluted area with the Particle Monte Carlo model coupled to the Model for Simulating Aerosol Interactions and Chemistry and evaluated three factors influencing particle CCN activity shortly after emission: (1) particle characteristics at the time of emission, (2) aging conditions near the emission source, and (3) the water vapor supersaturation at which CCN activity is evaluated. CCN concentrations were sensitive to particle properties at emission only under specific environmental conditions. Diesel emissions did not strongly influence local CCN concentrations at low cloud supersaturation thresholds ($s < 0.2\%$), regardless of particle characteristics at emission or aging conditions. At higher supersaturation thresholds ($s > 0.2\%$) and under conditions of rapid secondary aerosol formation, changes in CCN concentrations showed a greater sensitivity to particles' emission size than composition.

Citation: Fierce, L., N. Riemer, and T. C. Bond (2013), When is cloud condensation nuclei activity sensitive to particle characteristics at emission?, *J. Geophys. Res. Atmos.*, *118*, 13,476–13,488, doi:10.1002/2013JD020608.

1. Introduction

[2] The climate effects of anthropogenic aerosols remain one of the largest uncertainties in assessing human-induced climate change [*Anderson et al.*, 2003; *Forster et al.*, 2007]. Aerosols alter the Earth's energy balance directly by scattering and absorbing solar radiation [*Hansen and Sato*, 2001; *Boer and Yu*, 2003; *Takemura et al.*, 2005; *Kim and Ramanathan*, 2008] and indirectly through their interaction with clouds [*Twomey*, 1977; *Twomey et al.*, 1984; *Albrecht*, 1989; *Lohmann and Feichter*, 2005]. An increase in cloud condensation nuclei (CCN) from anthropogenic emissions may affect cloud radiative properties [*Twomey*, 1977; *Twomey et al.*, 1984] and cloud lifetime [*Albrecht*, 1989], known as the aerosol indirect effects. Greater CCN concentrations cause the cloud liquid water to be spread among more droplets, causing brighter clouds and a negative radiative forcing. Furthermore, the growth of CCN into cloud droplets and subsequent removal of aerosol mass when the cloud precipitates, termed nucleation scavenging, is an important removal mechanism for many aerosol species [*Cozic et al.*, 2007]. Therefore, the CCN activation properties of emitted particles affect the aerosol indirect effect, as well as the budget of many aerosol species.

[3] Primary particles are especially important in determining the aerosol number budget [*Chang et al.*, 2009; *Spracklen et al.*, 2010; *Reddington et al.*, 2011] and the associated increase in CCN concentrations [*Pierce and Adams*, 2009; *Spracklen et al.*, 2011]. Freshly emitted combustion particles are initially too small and hydrophobic to activate under most environmental conditions [*Weingartner et al.*, 1997; *Maricq*, 2007], but their properties are altered soon after emission by condensation of semivolatile substances and coagulation with preexisting particles [*Johnson et al.*, 2005]. This change in aerosol size and composition, termed "aging" [*Weingartner et al.*, 1997], increases particles' susceptibility to CCN activation [*Cantrell et al.*, 2001; *Hitzenberger et al.*, 2001; *Zuberi et al.*, 2005; *Andreae and Rosenfeld*, 2008; *Furutani et al.*, 2008]. The CCN activity of primary particles, therefore, depends on the properties of particles at emission, which for many sources are not well known [*Bond et al.*, 2004; *Sodeman et al.*, 2005; *Toner et al.*, 2006], and the aging processes that affect them after emission.

[1]Department of Civil and Environmental Engineering, University of Illinois at Urbana-Champaign, Urbana, Illinois, USA.
[2]Department of Atmospheric Sciences, University of Illinois at Urbana-Champaign, Urbana, Illinois, USA.

Corresponding author: N. Riemer, Department of Atmospheric Sciences, University of Illinois at Urbana-Champaign, Urbana, IL 61801, USA. (nriemer@illinois.edu)

2169-897X/13/10.1002/2013JD020608

[4] Although many of the microphysical properties governing CCN activity have been identified, there remains a lack of quantitative connection between particles as emitted and their ultimate effect on CCN concentrations. In particular, a deeper understanding of the rates and dominant factors governing transition between fresh emissions and CCN-active particles would enable effective parameterizations for global models. This work evaluates the sensitivity of primary particles' CCN activity to their size and composition at emission, and we evaluate how this sensitivity depends on the cloud supersaturation level and aging conditions near the emission source. We focus on particles emitted from a particular source, diesel engines, because they represent an important number fraction of particle emissions [*Lloyd and Cackette*, 2001] and because their CCN activity is important to understand their net forcing [*Stier et al.*, 2007; *Chen et al.*, 2010]. The lessons drawn from this particle type are also applicable to other hydrophobic primary aerosols.

[5] Modeling studies at the global scale show that carbonaceous aerosols have a strong influence on cloud radiative properties [*Chen et al.*, 2010; *Bauer et al.*, 2010; *Jacobson*, 2010; *Spracklen et al.*, 2011; *Koch et al.*, 2011] and that assumptions about particle characteristics at emission are a key uncertainty [*Bauer et al.*, 2010; *Spracklen et al.*, 2011; *Koch et al.*, 2011]. For example, *Koch et al.* [2011] compared the cloud radiative effects of fossil fuel and biomass burning aerosol emissions in six global models. On average, cloud microphysical effects led to a negative forcing approximately equal in magnitude but opposite in sign to the direct forcing by particles emitted from these sources. Biomass burning aerosol exerted a more negative indirect forcing than aerosol emissions from fossil fuels, which the authors attributed in part to differences in the microphysical properties of particles originating from these two sources. In these studies, biomass burning particles were initially more hygroscopic than fossil fuel particles, and, in some cases, biomass burning particles were emitted with a larger mean diameter. However, the geographic distribution of particle emissions also differs for biomass and fossil fuel sources. Cloud responses to particle emissions vary regionally because of variation in environmental conditions, so it is unclear whether differences in cloud response from biomass and fossil fuel emissions are caused by differences in particle microphysical properties or by differences in the regional distribution of each source.

[6] These global modeling studies included a number of cloud processes and were conducted on large spatial scales, with only a limited representation of aerosol properties, so these studies have not isolated the factors to which cloud-aerosol interactions are most sensitive. In this work, we complement the broad findings of global models by simulating the evolution of aerosols near the emission source using a detailed aerosol model that resolves the composition of each simulated particle. This work evaluates how aging conditions and environmental supersaturation levels affect the relationship between primary aerosol emissions and the number concentration of atmospheric CCN. We examine how two important aging processes, condensation and coagulation, affect the CCN activity of primary particles as a function of time after emission. The relative impact of these processes depends on particle size and composition, and we elucidate this behavior with sensitivity studies. The results of this sensitivity analysis can be used to identify the degree of detail in particulate emission properties required to predict CCN activity. In addition, this analysis will lead to a mechanistic understanding of how emissions affect CCN, cloud droplet number, and, ultimately, cloud forcing.

[7] The particle-resolved simulation of aerosol dynamics and methods for computing particle CCN activity are discussed in section 2. Particle aging mechanisms are analyzed for a single set of emission characteristics in section 3. The sensitivity of the CCN activity of aged particles to particle properties at emission is evaluated in section 4. Finally, discussion and conclusions are presented in section 5.

2. Methodology

[8] We simulate aerosol aging with a detailed aerosol microphysical model to evaluate how particle characteristics at emission and environmental conditions near the emission source influence CCN concentrations and aerosol removal by nucleation scavenging. We considered three factors: (1) size and composition of freshly emitted particles, (2) conditions for aging by condensation and coagulation near the emission source, and (3) water vapor supersaturation at which CCN activity is evaluated.

2.1. Particle-Resolved Simulation of Aerosol Aging

[9] Particle Monte Carlo model coupled to the Model for Simulating Aerosol Interactions and Chemistry (PartMC-MOSAIC) [*Zaveri et al.*, 2008; *Riemer et al.*, 2009] simulates the evolution of trace gases and individual aerosol particles in a well-mixed Lagrangian air parcel. The volume of the parcel is on the order of a few cubic centimeters in the simulations presented here, which is assumed to be representative of a much larger volume. Within the air parcel, the model tracks the mass composition of N_p simulated particles, where $N_p \approx 10^5$ discrete particles in the simulations presented in this work. Model calculations were performed using a time step of 60 s.

[10] As the simulation proceeds, the particle population is altered in two ways. First, each particle's mass composition evolves continuously by condensation and evaporation of semivolatile substances, processes that are simulated deterministically by MOSAIC. MOSAIC includes modules for gas-phase photochemistry [*Zaveri and Peters*, 1999], particle-phase thermodynamics [*Zaveri et al.*, 2005a, 2005b], and gas-particle mass transfer [*Zaveri et al.*, 2008]. The coupled model treats all atmospherically important aerosol species including sulfate (SO_4^{2-}), nitrate (NO_3^-), chloride (Cl^-), carbonate (CO_3^{2-}), ammonium (NH_4^+), sodium (Na^+), calcium (Ca^+), methanesulfonic acid (MSA), black carbon (BC), primary organic aerosol (POA), and a number of secondary organic aerosol (SOA) species.

[11] Second, particles are added to and removed from the simulation through aerosol emissions, dilution with background air, and coagulation events, processes that are simulated stochastically by PartMC. PartMC also tracks the source from which each particle originated. If two particles coagulate, the model stores the number of particles originating from each source that are contained within the combined particle. In this work, we pay special attention to the evolution of particles that contain at least one particle originating

Table 1. Aerosol Emissions and Initial Conditions for Base Case Simulation [*Riemer et al.*, 2009][a]

Initial/Background	N (m^{-3})	D_{gm} (μm)	σ_g	Composition by Mass	κ_{emit}
Aitken mode	3.2×10^9	0.02	1.45	50% $(NH_4)_2SO_4$, 50% POA	0.325
Accumulation mode	2.9×10^9	0.116	1.65	50% $(NH_4)_2SO_4$, 50% POA	0.325
Emissions	$\dot{N}_{emit}$ ($m^{-2}s^{-1}$)	$D_{gm,emit}$ (μm)	$\sigma_{g,emit}$	Composition by Mass	κ_{emit}
Meat cooking	9×10^6	0.0865	1.9	100% POA	0.001
Diesel vehicles	1.6×10^8	0.05	1.7	30% POA, 70% BC	3×10^{-4}
Gasoline vehicles	5×10^7	0.05	1.7	80% POA, 20%BC	8×10^{-4}

[a]The quantity κ_{emit} is the hygroscopicity parameter assigned to particles at emission.

from diesel exhaust. A detailed model description can be found in *Riemer et al.* [2009]. PartMC Version 2.1.4 was used to generate the results in this paper.

2.2. Urban Plume Scenario

[12] We present simulations of an air parcel advected through a large urban area based on the idealized plume scenario described in *Riemer et al.* [2009], with conditions similar to those of Los Angeles. The simulations started at 6:00 a.m., at which time the parcel contained only background gas and aerosol, and received gas and aerosol emissions from 6:00 a.m. until 6:00 p.m. After 6:00 p.m., all emissions were discontinued until the simulation ended at 6:00 a.m. the following morning. The parcel was mixed with background air according to a fixed dilution rate, and the temperature and mixing height varied according to a prescribed diurnal profile. The relative humidity varied as a function of temperature. The temperature peaked at 300 K in the middle afternoon, corresponding to a relative humidity of 55%. At night the temperature decreased to 290 K, and the relative humidity increased to 95%. Time series for selected trace gases and meteorologic conditions are given in *Riemer et al.* [2009].

[13] The size distribution and composition assigned to background and emitted particles in the baseline scenario are given in Table 1, including number-based geometric mean diameter ($D_{gm,emit}$) and standard deviation ($\sigma_{g,emit}$), the mass composition, and the effective hygroscopicity parameter (κ_{emit}) corresponding to that composition. The background aerosol consisted of Aitken and accumulation modes and was composed of $(NH_4)_2SO_4$ and POA. Three sources of carbonaceous aerosols were emitted: (1) diesel vehicle emissions, (2) gasoline vehicle emissions, and (3) meat cooking emissions. Although particles from diesel exhaust are the focus of this study, the other two sources were included to simulate a more realistic composition of urban aerosol. In this base case scenario, the number-based emission strength from diesel particulate emissions far exceeded number-based emission from any other source (Table 1). The size distribution parameters and composition of particle emissions were based on measurements from *Kittelson et al.* [2006a, 2006b] and *Eldering and Cass* [1996], respectively. The initial gas concentrations and gas emissions were adapted from the southern California Air Quality Study of *Zaveri et al.* [2008]. This plume scenario is not meant to represent any particular episode but was chosen to analyze changes in the aerosol mixing state under conditions simple enough that the dominant aging processes could be understood.

2.3. κ-Köhler Model for Computing Critical Supersaturation

[14] We determined CCN properties from the PartMC-MOSAIC model data by computing each simulated particle's critical supersaturation for CCN activation. The hygroscopicity parameter κ_i, introduced by *Petters and Kreidenweis* [2007], is defined for each particle by its effect on the water activity $a_{w,i}$ of the droplet solution. The effective hygroscopicity parameter for each particle (κ_i) is the volume-weighted average of the κ values of its constituent aerosol species. The values for κ assigned to each aerosol species simulated in this work are given in Table 2.

[15] The equilibrium saturation ratio S_i over an aqueous droplet of diameter D_i is given by the following:

$$S_i(D_i) = \frac{D_i^3 - D_{dry,i}^3}{D_i^3 - D_{dry,i}^3(1-\kappa_i)} \exp\left(\frac{4\sigma_w M_w}{RT\rho_w D_i}\right), \quad (1)$$

where σ_w is the surface tension of water, M_w is the molecular weight of water, R is the universal gas constant, T is the ambient temperature, ρ_w is the density of water, and $D_{dry,i}$ is the dry diameter of particle i.

[16] The critical wet diameter $D_{c,i}$ is the diameter D_i at which $S_i(D_i)$ is maximal. The critical supersaturation ratio $S_i(D_{c,i})$ is then computed by substituting $D_{c,i}$ into equation (1), and the critical supersaturation is given by $s_{c,i} = (S_i(D_{c,i}) - 1) \times 100$. Once $s_{c,i}$ for each particle is known, CCN-active particles at some threshold s are identified as those with a critical supersaturation less than or equal to the threshold ($s_{c,i} \leq s$).

Table 2. Hygroscopicity Parameter Assigned to Aerosol Species

Aerosol Species	κ	Citation
NO_3	0.65	*Clegg et al.* [1998], *Svenningsson et al.* [2006], and *Petters and Kreidenweis* [2007]
SO_4	0.65	*Clegg et al.* [1998], *Svenningsson et al.* [2006], and *Petters and Kreidenweis* [2007]
NH_4	0.65	*Clegg et al.* [1998], *Svenningsson et al.* [2006], and *Petters and Kreidenweis* [2007]
SOA	0.1	*Prenni et al.* [2007]
BC	0	*Petters et al.* [2006]
POA	0.001	*Petters et al.* [2006]

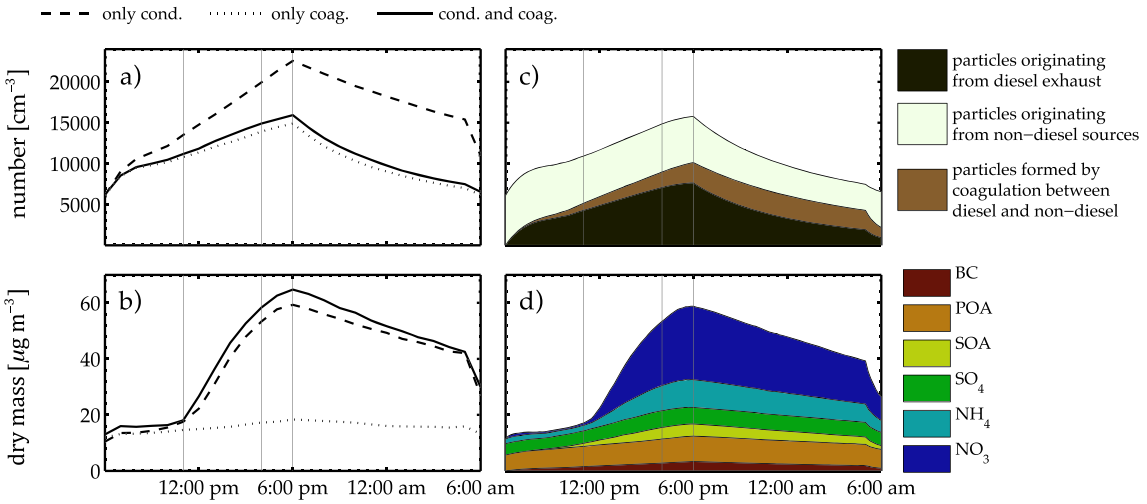

Figure 1. Evolution of (a) overall aerosol number concentration and (b) overall aerosol mass concentration for simulations representing different processes and, for only the simulation including both condensation and coagulation, the evolution of (c) aerosol number different classes of particles and (d) mass of aerosol species. Vertical lines show the time periods outlined in Table 3.

3. Evolution of CCN Activity in a Single Emission Scenario

[17] We first present results from a baseline emission scenario in order to illustrate the distinct roles of condensation and coagulation in altering the hygroscopic properties of particle emissions. Later, we show how differences in particle characteristics at emission influence their CCN activity after hours of aging. We determined the relative impact of each aging mechanism by comparing simulations under three limiting cases: (1) including condensation without coagulation, (2) including coagulation without condensation, and (3) including both condensation and coagulation. We then build on this analysis in section 4.1 to determine how each aging mechanism alters the sensitivity of CCN activity to particles' characteristics at emission.

[18] The temporal evolution of the aerosol number concentration and dry mass concentration is shown in Figures 1a and 1b, respectively, for each set of aging conditions. The particle number concentration changed by primary aerosol emissions, dilution with background air, and coagulation. Aerosol emissions and dilution also affect the aerosol mass concentration, which also evolves by condensation and evaporation of semivolatile substances. These processes all vary throughout the day.

[19] The diurnal variation in aging conditions consisted of four key time periods, which are outlined in Table 3. Early in the simulation (6:00 a.m. to 11:00 a.m.), particle emissions caused an increase in the number concentration and freshly emitted particles aged primarily by coagulation. The middle of the day (11:00 a.m. to 4:00 p.m.) was characterized by rapid condensation of ammonium nitrate, produced through photochemical reactions. Particles emitted after this period of rapid aging by condensation, but before emissions ceased (4:00 p.m. to 6:00 p.m.), did not experience rapid aging by condensation, so they remained hydrophobic unless they participated in a coagulation event. Dilution and coagulation were the dominant processes acting at night (6:00 p.m. to 6:00 a.m.), after emissions were discontinued and at a time when aging by condensation was slow.

[20] In this scenario, particles originating from diesel exhaust contributed a large fraction of the aerosol number concentration, shown in Figure 1c. The total number concentration is separated into three classes: (1) particles formed by coagulation between particles originating from diesel exhaust and particles originating from nondiesel sources, (2) particles emitted from diesel exhaust that had not coagulated with particles from other sources, and (3) particles originating from nondiesel sources that had not coagulated with particles from diesel exhaust. Categories 1 and 2 demonstrate how diesel particles influence the particle population and are the focus of this work. We refer to particles in categories 1 and 2 as "diesel particles," meaning particles that contain at least one particle originating from diesel exhaust. Note that category 1 includes only particles formed by intercoagulation between particles from diesel and nondiesel sources, so particles formed by coagulation between two particles from diesel exhaust are placed in category 2 and those formed by coagulation between particles from the background or nondiesel emission sources are placed in category 3.

Table 3. Time Periods Representing Aging Regimes

Time	Characteristics
6:00 a.m. to 11:00 a.m.	fresh particle emissions and slow aging by condensation
11:00 a.m. to 4:00 p.m.	fresh particle emissions and rapid aging by condensation of ammonium nitrate
4:00 p.m. to 6:00 p.m.	fresh particle emissions continue after condensational aging slows
6:00 p.m. to 6:00 a.m.	no particle emissions, and slow aging by condensation

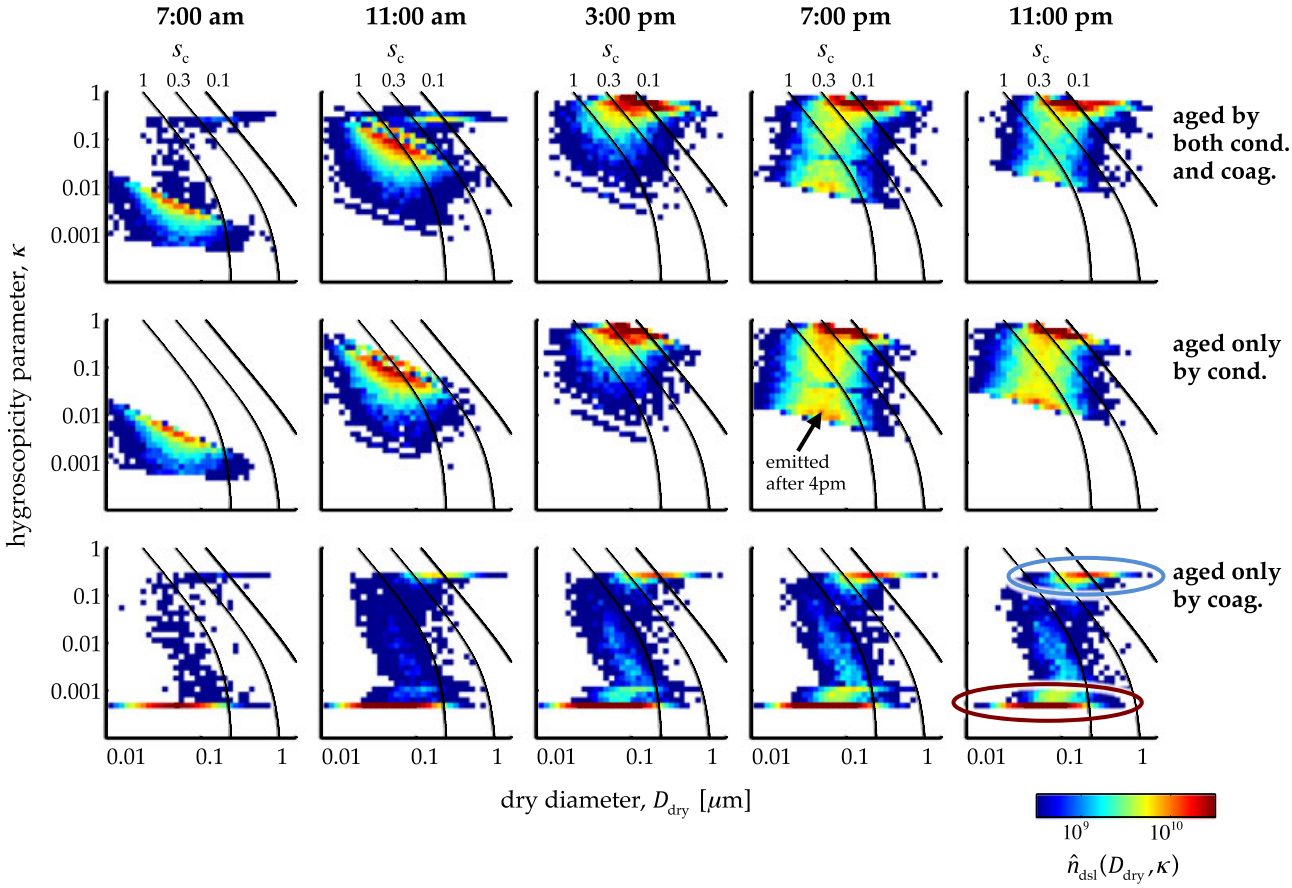

Figure 2. Two-dimensional normalized number distribution of diesel particles $\hat{n}_{dsl}(D_{dry},\kappa)$ shows how changes in size and hygroscopicity affect particles' critical supersaturation s_c (indicated by superimposed lines). The contribution of each aging mechanism to the full simulation is shown through comparisons between rows. The majority of particles acquire hygroscopic coating by condensation (middle), but some are instantaneously encompassed in CCN-active particles through coagulation events (indicated by the blue circle, bottom). In the absence of condensation, many particles remain unmodified throughout the simulation (indicated by the red circle).

[21] The mass concentration increased by approximately 50% from 6:00 a.m. until 6:00 p.m. because of primary particle emissions (BC and POA), shown in Figure 1d. The urban area simulated in this study contained high concentrations of nitric acid and ammonia, an average of 12 ppb and 1.7 ppb, respectively, leading to rapid formation of ammonium nitrate in simulations that include condensation. The aerosol mass concentration increased by more than a factor of 3 during the afternoon if condensation was simulated, from approximately 20 $\mu g\ m^{-3}$ at 12:00 p.m. to approximately 70 $\mu g\ m^{-3}$ at 6:00 p.m. Therefore, although coagulation was a key process influencing the aerosol number concentration, condensation was the most important process influencing the aerosol mass concentration. Beyond the 24 h, the number concentration was a factor of 2 greater when coagulation was not simulated (dashed line), and the mass concentration was underestimated by a factor of 2 at this time when condensation was neglected (dotted line).

3.1. Susceptibility to Nucleation Scavenging as a Function of Supersaturation

[22] Changes in particle characteristics that influence CCN activity are shown through a series of probability density distributions in Figure 2. At each time, the normalized two-dimensional distribution $\hat{n}_{dsl}(D_{dry},\kappa)$ is shown for each set of aging conditions. The unnormalized distribution $n_{dsl}(D_{dry},\kappa)$ is defined as follows:

$$n_{dsl}(D_{dry},\kappa) = \frac{\partial^2 N_{dsl}(D_{dry},\kappa)}{\partial \log D_{dry} \partial \log \kappa}, \quad (2)$$

where $N_{dsl}(D_{dry},\kappa)$ is the cumulative number distribution with respect to D_{dry} and κ. Because we compare particle populations with very different number concentrations, it is useful to use the normalized number distribution $\hat{n}_{dsl}(D_{dry},\kappa)$:

$$\hat{n}_{dsl}(D_{dry},\kappa) = \frac{n_{dsl}(D_{dry},\kappa)}{\int_{-\infty}^{\infty}\int_{-\infty}^{\infty} n_{dsl.}(D_{dry},\kappa) \mathrm{d}\log D_{dry} \mathrm{d}\log\kappa}. \quad (3)$$

[23] The individual contributions of condensation and coagulation are shown through comparisons between the simulation that includes both aging mechanisms (Figure 2, top) and simulations in which each mechanism operated alone (Figure 2, middle and bottom). The state of diesel particles is shown every 4 h from 7:00 a.m. until 11:00 p.m. The selected times were chosen to show how particle properties change during the key time periods outlined in Table 3.

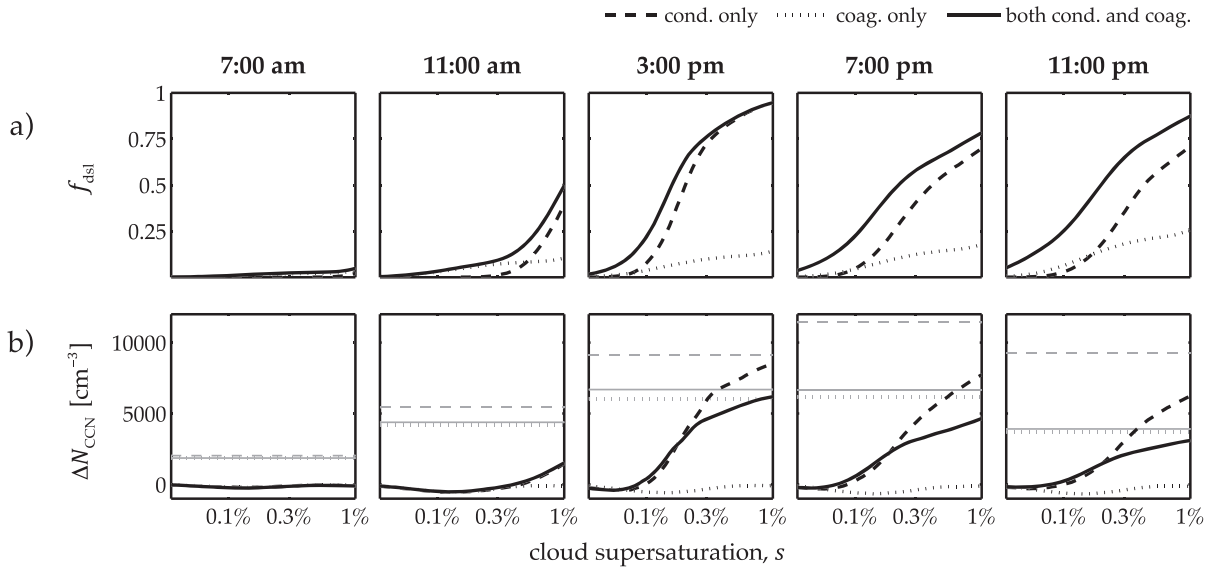

Figure 3. Evolution of (a) number fraction of diesel particles susceptible to nucleation scavenging, f_{dsl}, and (b) difference in CCN concentrations between simulations with and without diesel emissions, ΔN_{CCN}. The change in number concentration is indicated by the horizontal grey lines in Figure 3b.

[24] Curves of constant s_c for T = 293.15 K are plotted as a function of D_{dry} and κ in Figure 2. Particles that would be CCN active at a specified supersaturation s are those with $s_{c,i} \leq s$. Crossing the lines of constant s_c from left to right means that particles transition from CCN inactive to CCN active at that s. For the particle concentrations simulated in this paper, a cloud supersaturation of s = 0.1% is consistent with updraft velocities of 0.2–0.5 m s^{-1} (stratus clouds), and s = 0.6% is consistent with updraft velocities of 2–5 m s^{-1} (convective clouds).

[25] Each aging mechanism caused the evolution of the particle population to proceed in a different way. An hour after emissions started (7:00 a.m.), most diesel particles were too small and hydrophobic to activate at any $s < 1\%$. When particles aged only by condensation, $D_{dry,i}$ and κ_i increased incrementally over time as particles accumulated secondary aerosol coating, shown in Figure 2 (middle). Photochemical production of secondary aerosol between 11:00 a.m. and 4:00 p.m. caused rapid condensational aging during these hours. Particles emitted after 4:00 p.m. did not experience this rapid daytime aging and, consequently, remained small and hydrophobic with high values for $s_{c,i}$ throughout the night, shown in Figure 2 (middle).

[26] Without condensation $D_{dry,i}$ and κ_i were altered only for particles that participated in coagulation events, shown in Figure 2 (bottom). Because we assume that particles coagulate by Brownian motion, coagulation events occured most frequently between the largest and smallest particles in the distribution. The smallest diesel particles were often incorporated into much larger background particles through such coagulation events, forming a mode of diesel particles with κ_i approximately the same as the background (circled in blue in Figure 2). These combined particles were often CCN active at low values of s, enabling the removal of the small diesel particle contained in the combined particle through nucleation scavenging. The particles that did not participate in coagulation events maintained their initial hygroscopic properties throughout the simulation, shown by the mode of particles in Figure 2 (bottom) that maintain $\kappa_i = 3 \times 10^{-4}$ throughout the entire simulation (circle in red in Figure 2).

[27] As particles increase in size (greater $D_{dry,i}$) and hygroscopicity (greater κ_i), they become more susceptible to CCN activation and wet removal. The number fraction of diesel particles that are able to activate into CCN (f_{dsl}) is shown as a function of cloud supersaturation in Figure 3a. The value of $f_{dsl}(s)$ at a specific s is the portion of particles with $s_c \leq s$, corresponding to particles above that s_c line in Figure 2. Because f_{dsl} is related to the time-dependent number concentration of diesel particles, the same value of f_{dsl} at different times could have a very different effect on the number concentration of CCN.

[28] Freshly emitted particles were CCN active only at very high supersaturation levels ($s > 1\%$), but their CCN activity increased as they aged by condensation and coagulation. Condensation of semivolatile substances between 11:00 a.m. and 3:00 p.m. caused $s_{c,i}$ to decrease for all diesel particles (Figure 2), enabling their activation and removal under a greater range of cloud supersaturation levels. For simplicity, we discuss changes in the f_{dsl} spectrum using a single value, the supersaturation required to activate 50% of particles (s_{50}). While f_{dsl} at a specific time and supersaturation indicates the portion of particles that could be removed at that supersaturation (Figure 3a), the quantity s_{50} provides information on the f_{dsl} curve with only a single value. In simulations with only condensation (dashed lines) s_{50} decreased from $s_{50} \approx 1\%$ at 11:00 a.m. to $s_{50} \approx 0.3\%$ at 3:00 p.m. On the other hand, a small portion of diesel particles combined with hygroscopic particles through coagulation events, increasing $f_{dsl}(s)$ at $0.1\% < s < 1\%$ in simulations including coagulation without condensation (dotted lines of Figure 3a).

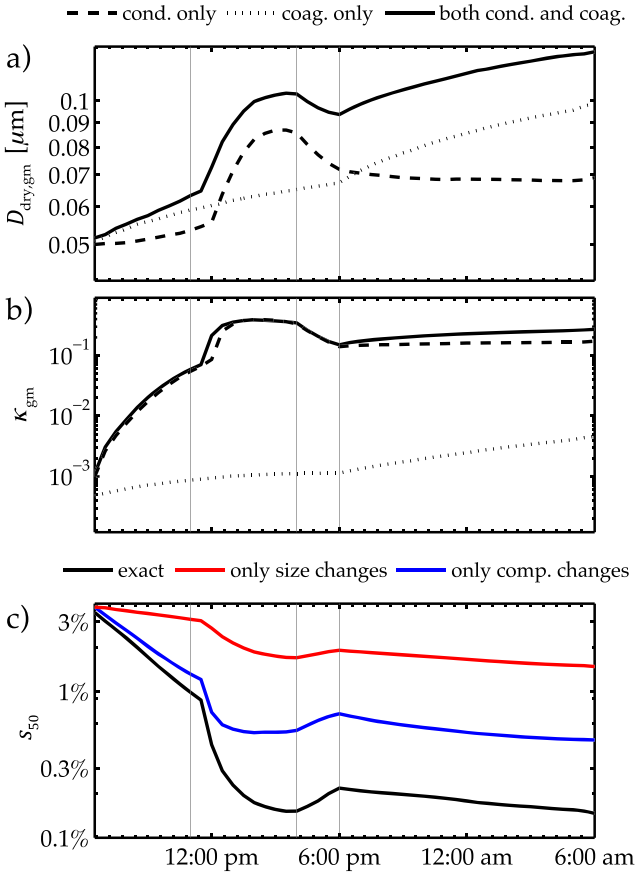

Figure 4. For each set of aging conditions, evolution of diesel particles' (a) geometric mean diameter and (b) geometric mean hygroscopicity parameter. For simulations including both condensation and coagulation, evolution of (c) supersaturation at which 50% of diesel particles become CCN active for exact PartMC-MOSAIC results (black line), assuming particles size changes but not their composition (red line) and assuming their composition changes but not their size (blue line). Vertical lines show the time periods outlined in Table 3.

3.2. CCN Concentrations as a Function of Supersaturation

[29] Although the changes in particle hygroscopic properties presented in section 3.1 increased particles' susceptibility to nucleation scavenging, in this section we show that, even after several hours of aging, particle emissions did not always increase the number concentration of CCN. Changes in CCN concentrations from particle emissions depended strongly on aerosol dynamics near the emission source. We evaluated the contribution of diesel emissions to overall CCN concentration (N_{CCN}) by comparing N_{CCN} between simulations with and without diesel emissions. The difference in CCN concentrations, ΔN_{CCN}, is shown in Figure 3b for each set of aging conditions. Diesel emissions caused an increase in the aerosol number concentration, regardless of aging conditions, but only in certain cases did this increase in aerosol number correspond to an increase in N_{CCN}.

[30] In the previous section, we showed that diesel particles often became encompassed in highly hygroscopic particles through coagulation events, increasing their susceptibility to removal through nucleation scavenging at $s < 0.2\%$. However, these small diesel particles did not form distinct CCN if they are incorporated in particles that were CCN active prior to the coagulation event. Unless condensation occurred, diesel particles that did not coagulate with background particles remained too hydrophobic to increase N_{CCN} at any $s < 1\%$ (Figure 3b). At high supersaturation values ($s > 0.2\%$), diesel emissions caused the greatest increase in N_{CCN} in the presence of condensation and the absence of coagulation, suggesting that diesel particles experienced sufficient growth by condensation to form new CCN at these high values of s. At low supersaturation thresholds ($s < 0.2\%$) N_{CCN} was nearly the same for simulations with or without diesel emissions, indicating that diesel emissions did not influence N_{CCN} at these low values of s.

3.3. Relative Importance of Changes in Size Versus Composition

[31] As discussed in section 3.1, the changes in CCN activation are the result of simultaneous changes in particles' dry diameter and hygroscopicity parameter. The evolution of diesel particles' geometric mean diameter ($D_{dry,gm}$) and geometric mean hygroscopicity parameter (κ_{gm}) are shown in Figures 4a and 4b, respectively. Changes in particle hygroscopicity were driven almost entirely by condensation (Figure 4b), while both condensation and coagulation were important in determining diesel particles' size distribution (Figure 4a).

[32] For the simulation including both condensation and coagulation, the relative importance of changes in size and composition on CCN activity are compared in Figure 4c. The supersaturation at which 50% of particles activate, s_{50}, is shown for (1) the population of diesel particles simulated by PartMC-MOSAIC, (2) the same particles but their initial composition and the modeled change in size, and (3) the same particles but with their initial size and the modeled change in composition.

[33] For the exact particle population from PartMC-MOSAIC (black line), s_{50} is approximately 3% at the start of the simulation, indicating that most particles are too hydrophobic to activate at relevant supersaturation levels. As particles increased in size (Figure 4a) and hygroscopicity (Figure 4b), s_{50} rapidly decreased. By 3:00 p.m., s_{50} was less than 0.2% (black line), corresponding to the shift in f_{dsl} shown in Figure 3a. If only changes in size were included (red line), s_{50} was an order of magnitude higher than for the exact simulation. On the other hand, if only particles' composition was modified, s_{50} was overpredicted by a factor of 3 (blue line). Both changes in size and hygroscopicity must be included to model CCN activity, and changes in hygroscopicity are particularly important.

[34] In summary, condensation caused the critical supersaturation of the majority of particles to decrease and, thereby, increased the number fraction susceptible to nucleation scavenging at high supersaturation thresholds ($s > 0.2\%$). The particles that aged by condensation also tended to increase N_{CCN}. On the other hand, coagulation increased particles' susceptibility to removal through nucleation scavenging at low s ($s < 0.1\%$), but diesel emissions did not lead to an increase in N_{CCN} at any $s < 1\%$ if aged by coagulation alone.

Table 4. Parameters Assigned to Diesel Emissions in Analysis of Sensitivity to Emission Size Distribution[a]

	Size Distribution Parameters		Composition				
Simulation	$D_{gm,emit}$ (μm)	$\dot{N}_{emit}$ ($m^{-2}s^{-1}$)	BC	POA	SO_4	κ_{emit}	$s_{50,emit}$
S1	0.025	1.28×10^9	70%	30%	0%	3×10^{-4}	8.3%
S2	**0.05**	$\mathbf{1.6 \times 10^8}$	**70%**	**30%**	**0%**	$\mathbf{3 \times 10^{-4}}$	**3.9%**
S3	0.1	2×10^7	70%	30%	0%	3×10^{-4}	1.9%
S4	0.2	2.5×10^6	70%	30%	0%	3×10^{-4}	0.9%

[a]The quantity $s_{50,emit}$ is the supersaturation at which 50% of freshly emitted particles activate. Bold font indicates baseline simulation.

4. Sensitivity of CCN Activity to Particle Size and Composition at Emission

[35] The properties of primary aerosol particles are determined partly by aging in the atmosphere, as discussed in the previous section, and partly by their characteristics at emission. In this section, we explore to what extent particle properties at emission influence their CCN activation properties after aging. We present a series of sensitivity simulations in which we varied the size distribution and composition of the particles at emission. Because the overall mass emission rate is typically better constrained than the assumed particle size distribution and composition, we performed and compared simulations for which the mass emission rate was the same but the microphysical properties of individual particles were varied.

[36] Results are presented for two sets of simulations, outlined in Tables 4 and 5. In scenarios S1–S4 (Table 4) diesel particles were emitted with the same composition in all scenarios (70% BC, 30% POA) and the emission size distribution was varied. To maintain the same mass emission rate while changing the particle size distribution, the number emission rate was varied accordingly. For example, doubling the geometric mean diameter of diesel emissions ($D_{gm,emit}$) reduced the number emission rate ($\dot{N}_{emit}$) by a factor of 8. In scenarios C1–C4 (Table 5), diesel emissions had the same size distribution in all four scenarios, and particle composition at emission was varied. Increasing the SO_4 content of emitted particles corresponded to an increase in their effective hygroscopicity parameter at emission (κ_{emit}) and a decrease in the critical supersaturation at which 50% of particles activate ($s_{50,emit}$). A particle's critical supersaturation for CCN activation ($s_{c,i}$) decreases as $D_{dry,i}$ or κ_i increases. Scenarios S2 and C1 are identical, corresponding to the baseline scenario that was presented in section 3.

4.1. Sensitivity of Nucleation Scavenging to Particle Characteristics at Emission

[37] The fraction of diesel particles able to activate into CCN, $f_{dsl}(s)$, is shown for scenarios S1–S4 and C1–C4 in Figure 5. As in the base case scenario, particles activated into CCN more easily after aging by condensation and coagulation. The temporal evolution of f_{dsl} at $s = 0.3\%$ is shown in Figure 5 (left) for simulations including both condensation and coagulation. At a single time, 11:00 p.m., results are shown as a function of supersaturation for each set of aging conditions. If differences between f_{dsl} at some s are large, then particles' susceptibility to CCN activation and their subsequent removal depends strongly on emitted particle properties at that s.

4.1.1. Scenarios S1–S4

[38] The evolution of $f_{dsl}(s)$ is shown for S1–S4 in Figure 5. All other factors being equal, particles with large diameters (e.g., S4) are able to activate at lower values of s than particles with small diameters (e.g., S1). Values for $f_{dsl}(s)$ at 7:00 a.m. show the characteristics of diesel particles when all emissions are fresh. The temporal evolution of $f_{dsl}(s)$ was influenced by the same processes outlined in Table 3.

[39] In all scenarios S1–S4, CCN activity increased for all particles as they aged by condensation (11:00 a.m. to 4:00 p.m.). Condensational aging caused the greatest changes in $f_{dsl}(s)$ for any given scenario, but, in the absence of coagulation, f_{dsl} for $0.1\% < s < 1\%$ remained sensitive to particles' emission size distribution after aging. In simulations that included coagulation without condensation, a portion of particles were encompassed in large background particles that were CCN active at $s < 0.1\%$, but many particles remained unaltered and hydrophobic. Aerosol properties evolved most rapidly and differences in CCN activity were smallest when the effects of both condensation and coagulation were included. In the simulations including both processes, the median critical supersaturation s_{50} initially ranged from 0.7% (S4) to 5.9% (S1) and decreased to the range of 0.08% (S4) to 0.18% (S1) after 24 h. Differences in s_{50} are discussed in further detail in section 4.1.3.

4.1.2. Scenarios C1–C4

[40] Although coagulation was important for decreasing the sensitivity of f_{dsl} to particles' emission size, condensation

Table 5. Parameters Assigned to Diesel Emissions in Analysis of Sensitivity to Emission Composition[a]

	Size Distribution Parameters		Composition				
Simulation	$D_{gm,emit}$ (μm)	$\dot{N}_{emit}$ ($m^{-2}s^{-1}$)	BC	POA	SO_4	κ_{emit}	$s_{50,emit}$
C1	**0.05**	$\mathbf{1.6 \times 10^8}$	**70%**	**30%**	**0%**	$\mathbf{3 \times 10^{-4}}$	**3.9%**
C2	0.05	1.6×10^8	68.6%	29.4%	2%	6.8×10^{-3}	2.3%
C3	0.05	1.6×10^8	63%	27%	10%	6.5×10^{-2}	1.3%
C4	0.05	1.6×10^8	35%	15%	50%	3.2×10^{-1}	0.6%

[a]Bold font indicates baseline simulation.

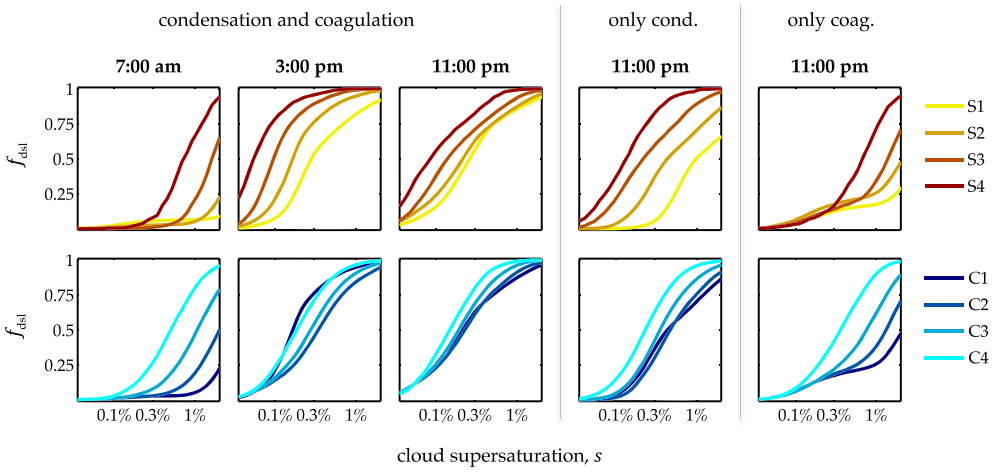

Figure 5. Fraction of particles susceptible to nucleation scavenging, f_{dsl}, as a function of cloud supersaturation s. Shown at 7:00 a.m., 3:00 p.m., and 11:00 p.m. for simulations including both condensation and coagulation and only at 11:00 p.m. for simulations of condensation only and coagulation only.

was the dominant process influencing sensitivities to particles' initial composition. At 7:00 a.m., when all diesel particles were fresh, f_{dsl} for C1–C4 was determined by particles' properties at emission, and s_{50} ranged from 0.5% to 3%. Particles that were initially hydrophobic (scenario C1) were unable to activate at relevant supersaturation thresholds ($s < 1\%$), but particles with substantial hygroscopic coating were CCN active at lower values of s. Particles' size and effective hygroscopicity parameter κ_i increased as they accumulated hygroscopic coating through condensation, and values of κ_i increased more rapidly when diesel emissions were initially hydrophobic (C1) than for particles emitted with some hygroscopic coating (C2–C4). By the time the simulations ended at 6:00 a.m. the following morning, s_{50} ranged from 0.1–0.2%, regardless of particles' initial hygroscopicity.

[41] In these simulations, s_{50} decreased to lower values for particles emitted without any SO_4 coating (C1) than particles emitted with 2% or 10% SO_4 by mass (C2 or C3, respectively). This is due to the combination of water uptake by the particles and the model treatment of ammonium nitrate on wet particles compared to dry particles. The current version of MOSAIC includes the Kelvin effect for wet particles but neglects it for dry particles, since the values for surface energies for the species of interest are unknown. Particles emitted between 9:00 a.m. and 4:00 p.m. in case C1 remained dry because they do not contain any SO_4 at emission, and the relative humidity during that time interval was below the deliquescence point of the inorganic mixture of ammonium, sulfate, and nitrate. During this time ammonium nitrate can form on the dry particles in C1 at a higher rate compared to the wet particles in cases C2–C3 since the Kelvin effect is neglected for dry particles.

[42] When coagulation was the only mechanism at work, f_{dsl} depended strongly on particles' initial composition throughout the simulation. Only particles that participated in coagulation events were altered under these conditions, so particles that did not coagulate maintained their initial hygroscopic properties throughout the simulation. The smallest emitted particles were likely to coagulate with much larger preexisting particles, increasing f_{dsl} at $s \approx 0.1\%$ in simulations including coagulation without condensation. Although aging by coagulation did ultimately reduce the dependence of s_{50} on particles' initial composition, in the absence of condensation many particles remained unaffected after hours of aging.

4.1.3. Sensitivity of Median Critical Supersaturation to Particle Characteristics at Emission

[43] As discussed in sections 4.1.1 and 4.1.2, the critical supersaturation at which 50% of particles activate, s_{50}, decreased in each scenario, indicating a shift in the f_{dsl} curve toward lower supersaturation levels and an increase in particles' susceptibility to nucleation scavenging. If differences in s_{50} between scenarios are large at some time, the supersaturation at which the majority of emitted particles activate depends strongly on particle characteristics at emission. We quantify how differences in s_{50} at emission ($s_{50,emit}$) affect differences in s_{50} throughout the simulation using the quantity Ψ. For example, Ψ is defined for scenarios S1–S4 as follows:

$$\Psi_S = \left| \frac{\left[s_{50}\right]_{S4} - \left[s_{50}\right]_{S1}}{\left[s_{50,emit}\right]_{S4} - \left[s_{50,emit}\right]_{S1}} \right|. \quad (4)$$

The corresponding sensitivity for scenarios C1 and C4 is given by Ψ_C. The end members of the scenarios (S1 and S4, C1 and C4) are always used when computing Ψ.

[44] The quantity s_{50} varies with time and depends on the emission scenario and the aging conditions, whereas $s_{50,emit}$ is a constant for each emission scenario and is independent of the aging conditions. If $\Psi_S = 1$, values for s_{50} differ between scenarios S1 and S4 as much as they did at the time of emission, although values for s_{50} may have decreased in each case. The other extreme, $\Psi_S = 0$, suggests that there is no difference in s_{50} between scenarios S1 and S4 and that particle emission properties do not influence their removal through nucleation scavenging after particles are processed in the atmosphere. The sensitivities Ψ_S or Ψ_C, therefore, indicate the degree to which differences in $s_{50,emit}$ translate to differences in s_{50} after aging.

[45] Figure 6 shows the time series for Ψ_S (red lines) and Ψ_C (blue lines). These quantities were computed for each

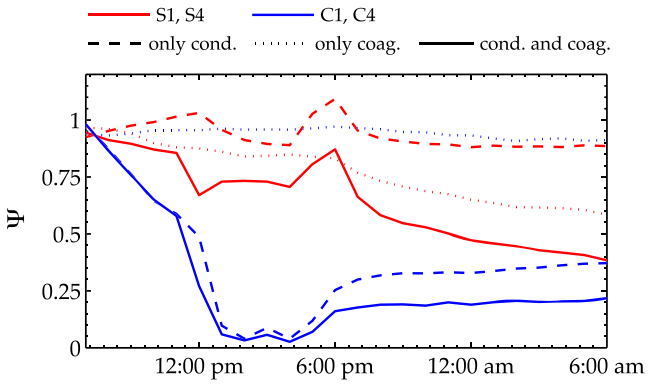

Figure 6. Time series of sensitivity parameters Ψ_S and Ψ_C. Differences between S1 and S4 are shown by red lines, illustrating the change in sensitivity to particles' emission size distribution, and differences between C1 and C4 are shown by blue lines, indicating the sensitivity to particles' composition at the time of emission. Results are shown for simulations including only the effects of condensation (dashed lines), only the effects of coagulation (dotted lines), and both condensation and coagulation (solid lines).

set of processing conditions. Values for Ψ_S and Ψ_C were lowest at all times when both processes were included, and simulations of each mechanism acting alone show which process was most influential in altering variability in s_{50} between scenarios.

[46] Early in the morning, values Ψ_S and Ψ_C were nearly equal to 1, indicating that the spread in s_{50} had not changed relative to $s_{50,emit}$. Photochemical reactions led to a period of rapid aging by condensation from 11:00 a.m. until 4:00 p.m.. During this time, the original difference in hygroscopicity between diesel particles in C1 and C4 was eliminated after particles were coated with condensing aerosol, causing Ψ_C to decrease to nearly 0 between 2:00 p.m. and 4:00 p.m. (solid and dashed blue lines). Although differences in chemical composition were rapidly eradicated by condensation, differences in size (quantified by Ψ_S) were altered much more slowly and were affected mostly by coagulation. Values for Ψ_S remained greater than 0.9 when coagulation was not included (dashed red line), but Ψ_S decreased to 0.25 after 24 h of simulation if coagulation was included in addition to condensation (solid red line).

[47] Coagulation was also important in altering the composition of particles emitted after sunset. Particles emitted after photochemical reactions ceased did not acquire a hygroscopic coating through condensation, so s_{50} varied more between C1 and C4 at 6:00 p.m. ($\Psi_C = 0.2$) than at 4:00 p.m. ($\Psi_C \approx 0$) for scenarios including only condensation or both condensation and coagulation (solid and dashed blue lines). If the effects of coagulation were included in addition to condensation, Ψ_C decreased to 0.1 by 6:00 a.m. the following morning (solid blue line); otherwise, Ψ_C remained at the value of 0.2 until the simulation ended (dashed blue line).

[48] In summary, the degree to which differences in particle microphysical properties at emission affect the mean CCN activation properties depends on the aging conditions near the emission source. Condensation rapidly altered particles' composition, such that s_{50} was insensitive to differences in particle composition at the time of emission ($\Psi_C \approx 0$). On the other hand, coagulation caused differences in s_{50} to decrease between particles emitted with different size distributions. As a result, coagulation caused Ψ_S to decrease to 0.35 after 24 h under conditions of rapid aging by both condensation and coagulation, whereas $\Psi_S \approx 1$ throughout the simulation if particles aged only by condensation.

4.2. Sensitivity of CCN Concentrations to Particle Characteristics at Emission

[49] Section 4.1 focused only on particles originating from diesel exhaust in order to evaluate the susceptibility of these particles to removal through nucleation scavenging. We now consider the entire particle population, including those from other sources, to evaluate differences in absolute CCN concentrations (ΔN_{CCN}) between simulations with and without diesel emissions. The temporal evolution of ΔN_{CCN} is shown at $s = 0.3\%$ for simulations including both condensation and coagulation in Figure 7 (left). For each set of aging conditions, results are shown as function of supersaturation at a single time, 11:00 p.m., in Figure 7 (right). These figures show how differences in aging conditions near the emission source affect the response in N_{CCN} to variation in particles' initial size distribution (S1–S4) and composition (C1–C4).

4.2.1. Scenarios S1–S4

[50] In scenarios S1–S4, total mass emission rates were identical, but the size distribution was varied, and particle number emission rates were adjusted accordingly. Although changes in the emission size distribution strongly influenced the aerosol number concentration, only under specific aging conditions did this increase in aerosol number lead to an increase in N_{CCN}. Diesel emissions did not strongly influence N_{CCN} at low supersaturation thresholds ($s < 0.2\%$), regardless of particle characteristics at emission or aging conditions near the emission source (Figure 7, right). At high supersaturation thresholds, fine particle emissions (S1–S2) caused large changes in N_{CCN} but required condensation aging to do so. In all cases, ΔN_{CCN} was not proportional to the change in aerosol number. For example, decreasing $D_{gm,emit}$ from the base case value of 0.05 μm (S2) to 0.025 μm (S1) corresponded to an increase in the number emission rate in scenario S1 by a factor of 8 and an increase in the number concentration by as much as a factor of 4, but N_{CCN} differed at most by a factor of 2 at even the highest values of s shown. Some emitted particles were lost through coagulation events, and others did not age sufficiently by condensation to activate. If the effects of coagulation were neglected, N_{CCN} differed by a factor of 6 between scenarios S4 and S1 at high supersaturation thresholds (e.g., $s = 1\%$).

[51] Fine particle emissions increased N_{CCN} less efficiently at low supersaturation threshold (e.g., $s = 0.1\%$), so there was less variability in ΔN_{CCN} between scenarios S1 and S4 at low s compared to high s. When the effects of coagulation were not simulated, emissions of the smallest diesel particles caused N_{CCN} to decrease by as much as 1000 cm^{-3} relative to simulations without diesel emissions. Particles present in high number concentrations competed for condensing aerosol, so a decrease in the aerosol number concentration by coagulation enhances the effects of

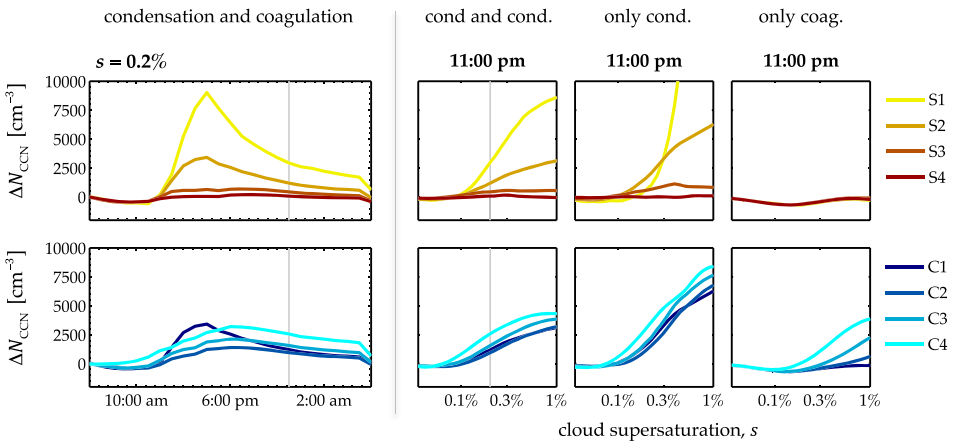

Figure 7. Difference in CCN concentrations between simulations with and without diesel emissions, ΔN_{CCN}, for scenarios (top) S1–S4 and (bottom) C1–C4. Results are shown as a function of time for a single cloud supersaturation, s = 0.2%, for simulations including both condensation and coagulation and are shown as a function of supersaturation at a single time, 11:00 p.m., for all aging conditions.

condensation. If both processes were simulated, emissions of fine particles resulted in a 500 cm^{-3} increase in N_{CCN} relative to simulations without diesel emissions. Therefore, although coagulation depletes the aerosol number concentration, causing a decrease in N_{CCN} at high values of s, the reduction in particle surface area by coagulation results in faster aging by condensation, causing an increase in N_{CCN} relative to simulations without coagulation at low values of s. In the absence of condensation, $\Delta N_{CCN} \approx 0$ for all s shown, regardless of particles' emission size distribution, so N_{CCN} was insensitive to diesel emissions for all $s < 1\%$.

4.2.2. Scenarios C1–C4

[52] Mass and number emission rates were the same for all scenarios C1–C4, so differences in N_{CCN} between scenarios were caused only by differences in per-particle solubility. After only a few hours of aging, diesel emissions caused an increase in N_{CCN} at $s > 0.1\%$ in all scenarios C1–C4. As established in section 4.1.2, particle CCN activation properties became less sensitive to their initial composition after hours of aging by condensation, and as a result N_{CCN} differed by less than 20% between scenarios C1 and C4 for any $0.1\% < s < 1\%$.

5. Discussion and Conclusions

[53] This study evaluates the importance of particles' emission size distribution and composition in predicting their CCN activity as they undergo aging in the atmosphere. We also compared the relative importance of the two aging processes, condensation and coagulation, and quantified how these findings depend on the environmental supersaturation at which CCN activity is evaluated. The results were first presented for a single emission scenario in section 3, in which particles were emitted with characteristics representing particles from diesel exhaust. We then analyzed how particles' size and composition at emission affect their CCN activity in section 4.

[54] The size distribution and composition of emitted particles affected their removal and their influence on CCN concentrations only under specific aging conditions. When evaluated at $s < 0.2\%$, diesel emissions yield little increase in N_{CCN}, regardless of particle characteristics at emission. At these low supersaturation thresholds, N_{CCN} differed by at most 5% between simulations with and without diesel emissions, as opposed to a factor of 2 difference in N_{CCN} at $s > 0.2\%$ for certain aging conditions. Therefore, N_{CCN} was sensitive to particles' emission characteristics only at $s > 0.2\%$, and under these conditions changes in N_{CCN} depended strongly on the aging mechanisms at work. Under regimes of rapid aging by condensation, N_{CCN} at $s > 0.2\%$ depended more strongly on particles' emission size distribution than on their composition at emission. On the other hand, if condensation was negligible, then particle emissions did not increase N_{CCN} at any s below 1% and N_{CCN} was insensitive to particle properties at emission.

[55] It is difficult to compare our process-level analysis, which isolates the influence of emission properties and environmental characteristics as causes of changing CCN on small scales, with global modeling results, which integrate changes over many conditions. Nevertheless, our results are broadly consistent with global modeling studies that evaluate the sensitivity of CCN concentrations to particle emissions. *Spracklen et al.* [2011] compared global model predictions of CCN against measurements and showed that carbonaceous aerosols must be included to adequately predict global CCN concentrations. We showed that particle emissions led to a twofold increase when environmental supersaturation was high enough ($s > 0.2\%$), but we add the finding that CCN concentrations are less affected at low supersaturation thresholds ($s < 0.2\%$) or in the absence of condensation. *Koch et al.* [2011] showed that changes in CCN concentrations from particle emissions depended on particles' emission source, suggesting a sensitivity of CCN concentrations to particle microphysical properties at emission. Our results are consistent with these global modeling results for environmental supersaturations above 0.2% when particles are aged under conditions of rapid secondary aerosol production, but we also find that N_{CCN} is insensitive to particles' initial characteristics at low supersaturations or in the absence of condensation.

[56] Where particle emissions did cause N_{CCN} to increase, there was a stronger sensitivity to the emission size distribu-

tion than the emission composition, consistent with global modeling studies that have identified the size distribution of aerosol emissions as a key uncertainty in the prediction of aerosol number concentrations and the associated CCN [*Pierce and Adams*, 2009; *Reddington et al.*, 2011]. We showed that varying the size distribution at emission caused large differences in the original aerosol number concentration, but changes in N_{CCN} were always smaller than changes in aerosol number.

[57] The composition of particle emissions did not strongly influence their CCN activity if particles were emitted prior to a rapid condensation event, which is consistent with measurements. For example, although the effective hygroscopicity parameter κ of fresh biomass burning emissions is known to differ between fuel types. *Engelhart et al.* [2012] showed that variability in κ decreased after particles aged by formation of secondary aerosol in a smog chamber. *Dusek et al.* [2006] showed that CCN activity of particles in remote regions depends strongly on particles' size distribution and is rather insensitive to particles' composition, consistent with the rapid changes in aerosol composition caused by condensation in this work. *Ervens et al.* [2010] modeled the CCN activity of aerosols measured at varying distances from pollution sources and found that far from emission sources CCN concentrations could be modeled with reasonable accuracy assuming the aerosol is a full internal, but near the emission source a more complex representation of aerosol mixing state was needed for agreement between measured and modeled CCN. Similarly, a different modeling study using PartMC-MOSAIC [*Zaveri et al.*, 2010] found that CCN activity could be modeled with high accuracy using a size-resolved rather than particle-resolved representation of the mixing state after only a few hours of aging by condensation. Consistent with these findings, we show that after a few hours of aging particles' CCN activation properties were more influenced by their initial size distribution than their initial composition. Differences in composition are important only near the emission source as long as particles experience a period of intense secondary aerosol formation.

[58] In this study, we evaluated sensitivities of CCN activity within 24 h after emission to particle characteristics at emission, a first step in isolating the importance of including particle microphysical properties in aerosol emission inventories. A complete evaluation of the influences of primary aerosol characteristics on CCN concentrations would include additional factors: the effects of differing environmental conditions, the evolution of particle characteristics after the 24 h of simulation, and the effects of heterogeneous reactions, such as photochemical oxidation and N_2O_5 hydrolysis.

[59] In summary, CCN concentrations were sensitive to particle microphysical properties at emission only under specific aging conditions. In all cases presented here, the number of CCN at $s < 0.2\%$ was insensitive to particles' emission size and composition. At $s > 0.2\%$, diesel emissions did increase CCN concentrations, and in this regime the number concentration of CCN was far more sensitive to particles' emission size than to composition. Only in the absence of secondary aerosol formation did differences in particles' initial composition influence their CCN activity after aging.

[60] **Acknowledgment.** This work was funded by National Aeronautics and Space Administration under grant NNX09AK66G.

References

Albrecht, B. (1989), Aerosols, cloud microphysics, and fractional cloudiness, *Science*, *245*(4923), 1227–1230.

Anderson, T., R. Charlson, S. Schwartz, R. Knutti, O. Boucher, H. Rodhe, and J. Heintzenberg (2003), Climate forcing by aerosols—A hazy picture, *Science*, *300*(5622), 1103–1104.

Andreae, M., and D. Rosenfeld (2008), Aerosol–cloud–precipitation interactions. Part 1. The nature and sources of cloud-active aerosols, *Earth Sci. Rev.*, *89*(1), 13–41.

Bauer, S., S. Menon, D. Koch, T. Bond, and K. Tsigaridis (2010), A global modeling study on carbonaceous aerosol microphysical characteristics and radiative effects, *Atmos. Chem. Phys.*, *10*(15), 7439–7456.

Boer, G., and B. Yu (2003), Climate sensitivity and response, *Clim. Dyn.*, *20*(4), 415–429.

Bond, T., D. Streets, K. Yarber, S. Nelson, J. Woo, and Z. Klimont (2004), A technology-based global inventory of black and organic carbon emissions from combustion, *J. Geophys. Res.*, *109*, D14203, doi:10.1029/2003JD003697.

Cantrell, W., G. Shaw, G. Cass, Z. Chowdhury, L. Hughes, K. Prather, S. Guazzotti, and K. Coffee (2001), Closure between aerosol particles and cloud condensation nuclei at Kaashidhoo Climate Observatory, *J. Geophys. Res.*, *106*, 28,711–28,718, doi:10.1029/2000JD900781.

Chang, L., S. Schwartz, R. McGraw, and E. Lewis (2009), Sensitivity of aerosol properties to new particle formation mechanism and to primary emissions in a continental-scale chemical transport model, *J. Geophys. Res.*, *114*, D07203, doi:10.1029/2008JD011019.

Chen, W., Y. Lee, P. Adams, A. Nenes, and J. Seinfeld (2010), Will black carbon mitigation dampen aerosol indirect forcing?, *Geophys. Res. Lett.*, *37*, L09801, doi:10.1029/2010GL042886.

Clegg, S., P. Brimblecombe, and A. Wexler (1998), Thermodynamic model of the system H^+-NH_4^+-SO_4^{2-}-NO_3^--H_2O at tropospheric temperatures, *J. Phys. Chem. A*, *102*(12), 2137–2154.

Cozic, J., B. Verheggen, S. Mertes, P. Connolly, K. Bower, A. Petzold, U. Baltensperger, and E. Weingartner (2007), Scavenging of black carbon in mixed phase clouds at the high alpine site Jungfraujoch, *Atmos. Chem. Phys.*, *7*(7), 1797–1807.

Dusek, U., et al. (2006), Size matters more than chemistry for cloud-nucleating ability of aerosol particles, *Science*, *312*(5778), 1375–1378.

Eldering, A., and G. Cass (1996), Source-oriented model for air pollutant effects on visibility, *J. Geophys. Res.*, *101*(D14), 19,343–19,369.

Engelhart, G., C. Hennigan, M. Miracolo, A. Robinson, and S. Pandis (2012), Cloud condensation nuclei activity of fresh primary and aged biomass burning aerosol, *Atmos. Chem. Phys.*, *12*, 7285–7293.

Ervens, B., et al. (2010), CCN predictions using simplified assumptions of organic aerosol composition and mixing state: A synthesis from six different locations, *Atmos. Chem. Phys.*, *10*, 4795–4807.

Forster, P., et al. (2007), Changes in atmospheric constituents and in radiative forcing, in *Climate Change 2007: The Physical Science Basis. Contribution of Working Group I to the Fourth Assessment Report of the Intergovernmental Panel on Climate Change*, edited by S. Solomon et al., pp. 129–234, Cambridge Univ. Press, Cambridge, United Kingdom.

Furutani, H., M. Dallosto, G. Roberts, and K. Prather (2008), Assessment of the relative importance of atmospheric aging on CCN activity derived from field observations, *Atmos. Environ.*, *42*(13), 3130–3142.

Hansen, J., and M. Sato (2001), Trends of measured climate forcing agents, *PNAS*, *98*(26), 14,778.

Hitzenberger, R., A. Berner, H. Giebl, K. Drobesch, A. Kasper-Giebl, M. Loeflund, H. Urban, and H. Puxbaum (2001), Black carbon (BC) in alpine aerosols and cloud water—Concentrations and scavenging efficiencies, *Atmos. Environ.*, *35*(30), 5135–5141.

Jacobson, M. (2010), Short-term effects of controlling fossil-fuel soot, biofuel soot and gases, and methane on climate, arctic ice, and air pollution health, *J. Geophys. Res.*, *115*(D14), D14209, doi:10.1029/2009JD013795.

Johnson, K., B. Zuberi, L. Molina, M. Molina, M. Iedema, J. Cowin, D. Gaspar, C. Wang, and A. Laskin (2005), Processing of soot in an urban environment: Case study from the Mexico City Metropolitan Area, *Atmos. Chem. Phys.*, *5*, 3033–3043.

Kim, D., and V. Ramanathan (2008), Solar radiation budget and radiative forcing due to aerosols and clouds, *J. Geophys. Res.*, *113*, D02203, doi:10.1029/2007JD008434.

Kittelson, D., W. Watts, and J. Johnson (2006a), On-road and laboratory evaluation of combustion aerosols—Part 1: Summary of diesel engine results, *J. Aerosol Sci.*, *37*(8), 913–930.

Kittelson, D., W. Watts, J. Johnson, J. Schauer, and D. Lawson (2006b), On-road and laboratory evaluation of combustion aerosols—Part 2: Summary of spark ignition engine results, *J. Aerosol Sci.*, *37*(8), 931–949.

Koch, D., et al. (2011), Soot microphysical effects on liquid clouds, a multimodel investigation, *Atmos. Chem. Phys.*, *11*(3), 1051–1064.

Lloyd, A., and T. Cackette (2001), Diesel engines: Environmental impact and control, *J. Air Waste Manage. Assoc.*, *51*(6), 809–847.

Lohmann, U., and J. Feichter (2005), Global indirect aerosol effects: A review, *Atmos. Chem. Phys.*, *5*(3), 715–737.

Maricq, M. M. (2007), Chemical characterization of particulate emissions from diesel engines: A review, *J. Aerosol Sci.*, *38*(11), 1079–1118.

Petters, M., and S. Kreidenweis (2007), A single parameter representation of hygroscopic growth and cloud condensation nucleus activity, *Atmos. Chem. Phys.*, *7*(8), 1961–1971.

Petters, M., A. Prenni, S. Kreidenweis, P. DeMott, A. Matsunaga, Y. Lim, and P. Ziemann (2006), Chemical aging and the hydrophobic-to-hydrophilic conversion of carbonaceous aerosol, *Geophys. Res. Lett.*, *33*, L24806, doi:10.1029/2006GL027249.

Pierce, J., and P. Adams (2009), Uncertainty in global CCN concentrations from uncertain aerosol nucleation and primary emission rates, *Atmos. Chem. Phys.*, *9*, 1339–1356.

Prenni, A., M. Petters, S. Kreidenweis, P. DeMott, and P. Ziemann (2007), Cloud droplet activation of secondary organic aerosol, *J. Geophys. Res.*, *112*, D10223, doi:10.1029/2006JD007963.

Reddington, C., et al. (2011), Primary versus secondary contributions to particle number concentrations in the european boundary layer, *Atmos. Chem. Phys.*, *11*, 12,007–12,036.

Riemer, N., M. West, R. Zaveri, and R. Easter (2009), Simulating the evolution of soot mixing state with a particle-resolved aerosol model, *J. Geophys. Res.*, *114*, D09202, doi:10.1029/2008JD011073.

Sodeman, D., S. Toner, and K. Prather (2005), Determination of single particle mass spectral signatures from light-duty vehicle emissions, *Environ. Sci. Technol.*, *39*(12), 4569–4580.

Spracklen, D., K. Carslaw, U. Pöschl, A. Rap, and P. Forster (2011), Global cloud condensation nuclei influenced by carbonaceous combustion aerosol, *Atmos. Chem. Phys*, *11*(17), 9067–9087.

Spracklen, D. V., et al. (2010), Explaining global surface aerosol number concentrations in terms of primary emissions and particle formation, *Atmos. Chem. Phys*, *10*(10), 4775–4793.

Stier, P., J. Seinfeld, S. Kinne, and O. Boucher (2007), Aerosol absorption and radiative forcing, *Atmos. Chem. Phys*, *7*(19), 5237–5261.

Svenningsson, B., et al. (2006), Hygroscopic growth and critical supersaturations for mixed aerosol particles of inorganic and organic compounds of atmospheric relevance, *Atmos. Chem. Phys*, *6*(7), 1937–1952.

Takemura, T., T. Nozawa, S. Emori, T. Nakajima, and T. Nakajima (2005), Simulation of climate response to aerosol direct and indirect effects with aerosol transport-radiation model, *J. Geophys. Res.*, *110*, D02202, doi:10.1029/2004JD005029.

Toner, S., D. Sodeman, and K. Prather (2006), Single particle characterization of ultrafine and accumulation mode particles from heavy duty diesel vehicles using aerosol time-of-flight mass spectrometry, *Environ. Sci. Technol.*, *40*(12), 3912–3921

Twomey, S. (1977), The influence of pollution on the shortwave albedo of clouds, *J. Atmos. Sci.*, *34*, 1149–1152.

Twomey, S., M. Piepgrass, and T. Wolfe (1984), An assessment of the impact of pollution on global cloud albedo, *Tellus B*, *36*(5), 356–366.

Weingartner, E., H. Burtscher, and U. Baltensperger (1997), Hygroscopic properties of carbon and diesel soot particles, *Atmos. Environ.*, *31*(15), 2311–2327.

Zaveri, R. A., J. C. Barnard, R. C. Easter, N. Riemer, and M. West (2010), Particle-resolved simulation of aerosol size, composition, mixing state, and the associated optical and cloud condensation nuclei activation properties in an evolving urban plume, *J. Geophys. Res.*, *115*, D17210, doi:10.1029/2009JD013616.

Zaveri, R., R. Easter, J. Fast, and L. Peters (2008), Model for Simulating Aerosol Interactions and Chemistry (MOSAIC), *J. Geophys. Res.*, *113*, D13204, doi:10.1029/2007JD008782.

Zaveri, R., R. Easter, and L. Peters (2005a), A computationally efficient Multicomponent Equilibrium Solver for Aerosols (MESA), *J. Geophys. Res.*, *110*, D24203, doi:10.1029/2004JD005618.

Zaveri, R., R. Easter, and A. Wexler (2005b), A new method for multicomponent activity coefficients of electrolytes in aqueous atmospheric aerosols, *J. Geophys. Res.*, *110*, D02201, doi:10.1029/2004JD004681.

Zaveri, R., and L. Peters (1999), A new lumped structure photochemical mechanism for large-scale applications, *J. Geophys. Res.*, *104*(D23), 30,387–30,415.

Zuberi, B., K. Johnson, G. Aleks, L. Molina, M. Molina, and A. Laskin (2005), Hydrophilic properties of aged soot, *Geophys. Res. Lett.*, *32*, L01807, doi:10.1029/2004GL021496.